Indian Journal of Pure & Applied Physics
Vol. 64, November 2026, pp. 1216-1229
DOI: 10.56042/ijpap.v64i11.31872

Enhancing SRM Drive Performance in Solar-Roof EVs Using Advanced DITC Techniques

Ravikant Kumar*, Umesh Kumar Sinha & Ravi Bhushan

Department of Electrical Engineering, National Institute of Technology, Jamshedpur 831 014, India

Received: 23rd May 2026; accepted: 30th June 2026

This paper presents a dynamic system model of a solar-roof-integrated electric vehicle equipped with a switched reluctance motor drivetrain. A 2×2 photovoltaic array (813 W at 1000 W/m²) mounted on the vehicle roof is interfaced to a Li-ion battery pack (546 Ah, 48 V) through a Zeta DC-DC converter governed by an Incremental Conductance (INC) Maximum Power Point Tracking (MPPT) algorithm, which reduces output current and voltage ripple by up to 40 % relative to the raw PV output. The Advanced Direct Instantaneous Torque Control (ADITC) replaces the conventional hysteresis switching of DITC with a PWM duty-ratio strategy, reducing torque ripple to 11.62 % at rated load and 12.47 % at light load compared with 32.39 % for standard DTC under identical conditions. The solar roof reduces the battery state-of-charge discharge rate from 0.00444 % to 0.00368 % per second, extending the EV range by approximately 1 hour 2 minutes (20.66 %) per full discharge cycle. The SRM accelerates to 4000 rpm within 1.5–2.0 seconds under all load conditions. Simulation results are validated on an OPAL-RT OP4512 real-time simulator, confirming a 59.68 % reduction in torque ripple compared with conventional DTC.

Keyboard: Switch reluctance motor, Solar roof, Maximum power point, Zeta converter, Electric vehicle system, State of charge, Advance direct instantaneous torque control

1 Introduction

Current research is focused on improving efficiency and protecting our beautiful environment due to humanity's growing transportation needs. Solar-powered electric vehicles integrate solar panels into their designs, harnessing sunlight to charge their batteries or power auxiliary systems. While the solar contribution typically supplements charging rather than replacing traditional plug-in charging, it offers an eco-friendly innovation. The rapid uptake of electric vehicles (EVs) is being driven by the need to reduce carbon emissions and dependency on fossil fuels, which is changing the face of transportation worldwide[1]. The incorporation of solar roofs, a state-of-the-art feature that uses renewable solar energy to supplement the vehicle's battery system, is one of the most recent advancements in EV technology. One innovative solution to increase energy efficiency and lessen dependency on traditional charging infrastructure is the incorporation of solar panels into electric vehicles. The design, use, and advantages of PV-integrated EVs are examined in this research, with an emphasis on how they can increase vehicle range, reduce emissions of carbon, and encourage the use of renewable sources. Important issues and potential paths for this technology are also covered[2].

Photovoltaic (PV) panels that are smoothly integrated into the vehicle's surface, usually the roof, make up solar roofs. The electrical energy produced by these panels can be utilised to run auxiliary systems or charge the car's battery[3]. In addition to increasing the vehicle's efficiency, this integration offers a sustainable way to increase its range, particularly in regions with lots of sunlight. cars with solar roofs are a big step towards attaining sustainable mobility by fusing the advantages of electric cars, such zero tailpipe emissions, energy efficiency, and lower running costs, with the self-sustaining potential of solar energy[4]. The possibility for lighter materials, improved energy management systems, and higher solar conversion efficiency as technology develops should make this breakthrough even more significant. The growing popularity of electric vehicles has highlighted the need for clean and efficient energy solutions. Traditional EVs use grid electricity, which may come from non-renewable sources, to charge their batteries. When PV systems are directly integrated with electric vehicles solar energy can be used to increase battery charge and reduce dependency on external power sources[5]. This essay

*Corresponding author: E-mail: kumar.ravikant94@gmail.com

proposes and evaluates the potential of a PV-integrated EV idea in light of recent technological advancements[6].

Solar-equipped EVs are expected to be crucial in hastening the world's shift to a cleaner and more sustainable future, whether for long-distance driving, daily commuting, or lowering reliance on external charging infrastructure. The solar roof EV versions are particularly advantageous in areas with plenty of sunlight because they are made to partially or completely charge their batteries using sunlight. EVs with solar roofs have been presented by innovative manufacturers like Tesla, Hyundai, and Light-year, demonstrating state-of-the-art designs and technologies intended to improve energy efficiency and lower overall energy costs. EVs with solar roofs are a big step towards a more sustainable and greener future by fusing clean energy production with zero-emission electric mobility.

Because of its exceptional fault tolerance and speed regulation capabilities, SRMs Motors have been the subject of much research. Figure 1 shows that EV set up with connected wheels, SRMs' application in electric vehicles has drawn a lot of attention. Since internal combustion engine (ICE) power reduces range anxiety problems for frequent travellers, hybrid electric vehicles provide us a viable answer to the need for emission-free transportation and satisfy the demands of longer travel. In terms of cost and dependability, SRM technology presents a viable substitute for EV applications. Even though there are technical obstacles, control strategies and materials science are becoming more viable due to continuous study and development[7]. They are especially appealing for mass-market EVs where cost is a crucial consideration because they don't require permanent magnets.

The success of SRM adoption in EVs will depend on how well the noise and control problems are resolved while maintaining the inherent cost and reliability advantages[8]. As production methods and control technology advance, SRM motors should become more competitive in the EV industry. For an SRM EV, a hybrid energy source consisting of a battery bank and super capacitor coupled in parallel via an Advance Zeta converter is intended to optimise efficiency in both motoring and braking modes and to meet storage and power flow requirements based on vehicle requirements[9]. A three-phase SRM drive has built-in charging and driving capabilities, which makes it more susceptible to potential drive defects even though it requires fewer switches to operate. Switching reluctance motors are therefore suggested as a substitute. Switched reluctance motor drives are becoming more and more popular in the EVs applications. due to their remarkable torque-speed characteristics, ease of control, robust and simple construction, and capacity to function dependably in the face of failure. Interestingly, SRMs have a simple rotor design without any brushes, commutators, windings, or magnets. Compared to other motor drive types seen in electric vehicles system, SRM drives are said to be superior. These days, SRM drives are appropriate for EV applications[10]. A simulation model for SRM driving is suggested by the study Describes the details of SRM displays the modelling of the SRM drive, followed by a helpful MATLAB simulation[11]. Provides the simulation results for the behaviour of the model. Lastly, it offers concluding remarks. Change the Reluctance This motor uses reluctance torque to function as a stepper motor[12]. The rotor's winding is removed to simplify the mechanical type. However, functioning is made more difficult by the incorporation of electronic components.

The direction of torque production in SRM is reluctance reduction direction. The converter or drive circuit and the control torque system regulate the torque production of each phase, which is

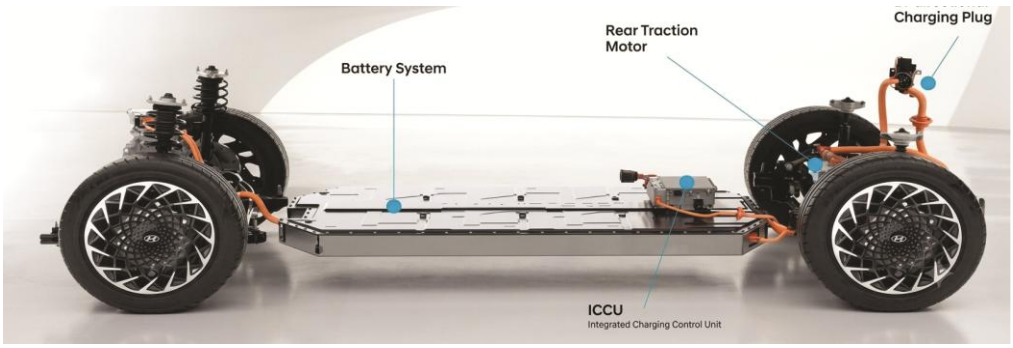

Fig. 1 — Electrical global modular platform

proportional to the square of its phase current[13]. The torque control method and drive circuit have a direct impact on the SRM's functionality and performance. As a result of on-going research, numerous topologies with fewer power switches, faster excitation and demagnetisation, high power factor, high efficiency, and high power have been developed[14]. With every new topology, there has historically been a trade-off between gaining some benefits and sacrificing some. The torque increases in proportion to the square of the current and the slope of the inductance. Given that the no matter which way the current flows, torque can be produced because it is proportional to the square of the current. Additionally, a negative torque zone is created based on the rotor position since the slope of the inductance alters the polarity of torque[15]. The rotor position angle and switching excitation must be in sync for there to be a motoring torque.

2 The Framework of Proposed Model

The design and operation of a PV-integrated EV that uses solar energy to augment its battery system and lessen reliance on grid electricity are described in this model. The car installs high-efficiency solar panels on its hood, roof, and other suitable spots. Lithium-ion battery packs to store grid and photovoltaic energy. A sophisticated control system to maximize the energy transfer between the electric drivetrain, battery, and PV panels.

In Fig. 2, this suggested dynamic model is displayed. It worked to lessen torque ripple, and when the EV motor is operating at full load or half load of the EV SRM motor, the speed is really smooth. The torque ripple can be managed and the SRM motor's performance improved by employing the Advanced Direct Instantaneous Torque Control (ADITC) approach.

2.1 Solar Roof Design by PV Panels

EV cars' roofs and other external surfaces are equipped with highly efficiency solar panels. MPPT controllers maximise energy production under a range of solar conditions[16]. Figure 3 showed the equivalent circuit diagram of PV solar system. A group of PV cells driven by a PV module is called a PV array. Different PV cells coupled in parallel and series make up a PV array. Growing current is caused by a parallel connection, while growing voltage is caused by a series connection[17].

Table 1 represents the PV array parameters for design a maximum power of solar cell is 813W power generation at 1000 irradiance and constant 25 ^{0}C.

Table 1 — A design of PV Array parameters

Parameters	Value
Current at MPP	7.83A
Short-circuit current	8.321A
Series resistant	0.193 Ω
String	2S *2P
Shunt resistant	330.659 Ω
Maximum power of model	813W
Voltage at open circuit	36.84V
Cell per module	60
Voltage at MPP	30.72V

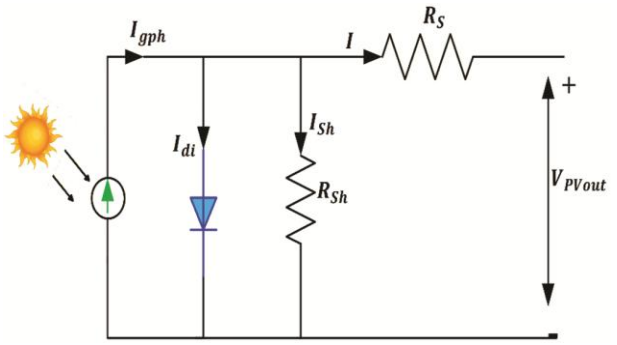

Fig. 3 — The basic equivalent circuit design of solar cells

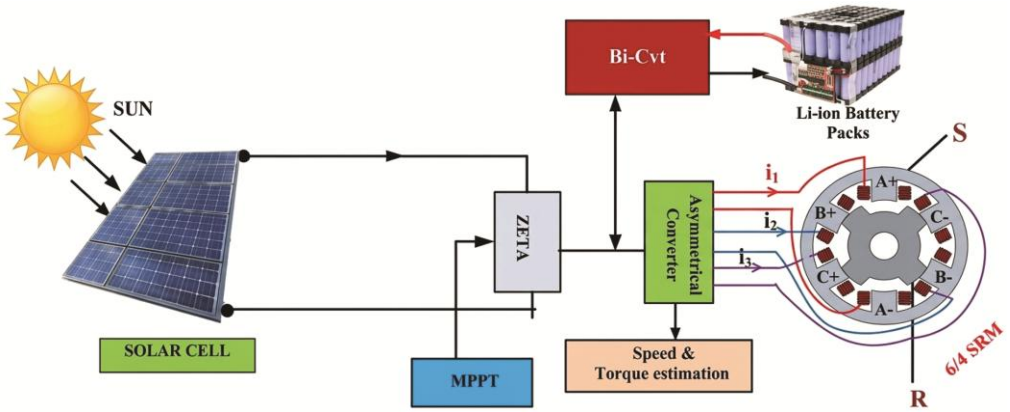

Fig. 2 — Proposed model of PV integrated EVs dynamic system

The equivalent circuit of PV array is composed of diode D, phase current source I_{Ph}, series resistance denoted $R_{S,}$ and parallel resistance R_{Sh} from P-N junction leakage. A solar-powered photovoltaic design the graph shows in Fig. 4 the PV array performance its characteristics current and power graph w.r.t voltage. Then the output current is;

$$I = I_{Ph} + I_{di} + I_{Sh} \quad \ldots (1)$$

2.2 Maximum Power Achieved by PV Array Using MPPT

In order to maintain the PV system functioning at or close to the highest peak power point of the PV panels under a variety of conditions, including varying solar irradiation and temperature, the MPPT algorithm continuously adjusts the impedance thought by the solar array. The control framework of an EV motor using MPPT algorithms is commonly used in the development of PV system controllers, as shown in Fig. 5. The algorithms take temperature and varying irradiance into consideration to guarantee that the PV system continuously generates the maximum amount of electricity. The MPPT technique guarantees that the PV array always generates the highest amount of power possible because data PV

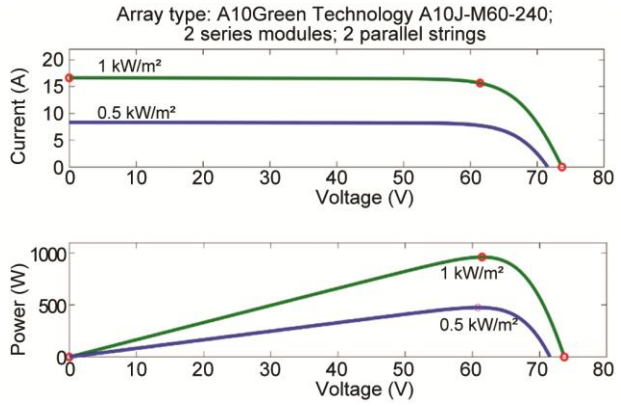

Fig. 4 — The selected PV array model the current and power response w.r.t. voltage

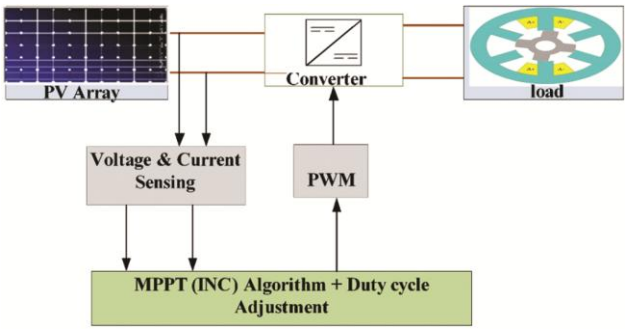

Fig. 5 — Block diagram MPPT of PV power generating systems

arrays are non-linear[18]. The popular basic techniques MPPT are P&O, INC, and incremental resistance due to their straightforward structure and simplicity of use. The P&O and INC algorithm suggestion is the result of the limited mark size of the algorithms' response to sudden changes in load resistance or solar irradiation conventional MPPT efficiency for the completed photovoltaic array[19]. In these systems, the inverter determines how much current travels through each module in the string (series). This architecture implies that certain modules will operate below their MPP, which will result in a drop, because different components have different P-V curves and MPP.

2.2.1 INC MPPT Algorithm

The INC approach uses the PV array's Incremental Conductance (IC) to calculate the MPP. The P&O algorithm shows a zero value at the MPP when analysing the PV array's voltage curve versus power, which means this method requires more computing resources from the controller but responds more quickly to changing conditions[20]. By comparing the IC with the array conductance, the INC algorithm calculates the maximum power.

To forecast the effects of a voltage modification, the INC approach employs small variations in PV array voltage and current. This approach follows changing conditions faster than the P&O algorithm, but it also requires more computing power from the controller. Similar to the P&O approach, it may result in variations in output power. In this method, incremental conductance is employed. Use the PV array's ΔI/ΔV to determine the sign of the power variation with regard to (ΔP/ΔV) to voltage[21]. By comparing the array conductance, I/V with the incremental conductance $\Delta I/\Delta V$, the INC method determines the maximum power point. Upon reaching $\Delta I/\Delta V = I/V$, the voltage is the MPP voltage. It is maintained by the controller until the irradiation changes and the process is repeated. $P = VI$ and $\Delta P/\Delta V = 0$ at the maximum power point are assumed in the INC approach[22]. The PV device's output voltage and current are determined by the IC technique. The INC algorithm's implementation flowchart is displayed in Fig. 6. The following comparable mathematical equation provides an explanation of the INC algorithm.

In INC algorithm MPP technique show in a flow chart is executed in MATLAB function. The following is an expression for the source's output power;

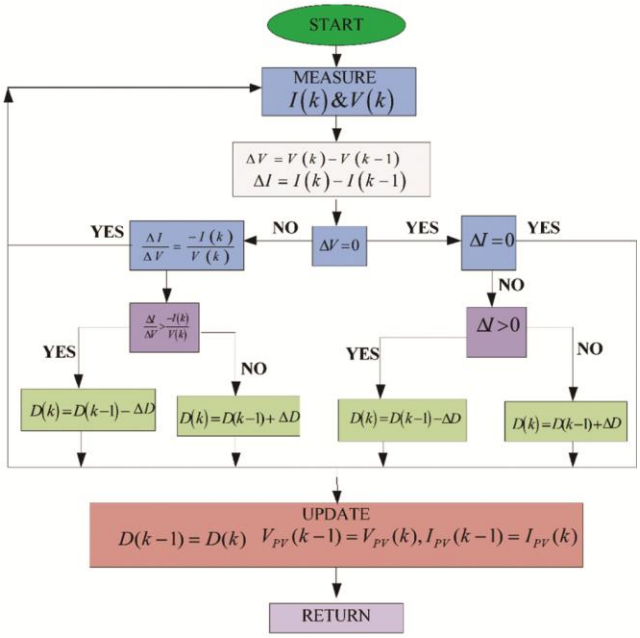

Fig. 6 — The flowchart of the INC MPPT algorithm

$$P = V * I \quad \ldots (2)$$

The chain approach for product derivatives in relation to voltage yield;

$$\frac{\Delta P}{\Delta V} = \frac{\Delta(VI)}{\Delta V} \quad \ldots (3)$$

$$= \frac{I\Delta V}{\Delta V} + \frac{V\Delta I}{\Delta V}$$

$$\left(\frac{I}{V}\right) * \frac{\Delta P}{\Delta V} = \left(\frac{I}{V}\right) + \frac{\Delta I}{\Delta V} \quad \ldots (4)$$

A source's output voltage is typically positive. Therefore, this algorithm's primary goal is to find the voltage operating point where the conductance equals the incremental conductance. The INC algorithm is determined by the slope of the P-V curve, which is expressed by equation (5–7). The slope will be zero at MPP, rising (+Ve) on the left and lowering (-Ve) on the right.

The following are the algorithm's fundamental equations;

$$\text{If; } \frac{\Delta I}{\Delta V} = \frac{I}{V} \quad \ldots (5)$$

The output voltage is;

$$\frac{\Delta I}{\Delta V} > -\frac{I}{V} \text{ On the LHS of MPP} \quad \ldots (6)$$

$$\frac{\Delta I}{\Delta V} < -\frac{I}{V} \text{ On the RHS of MPP} \quad \ldots (7)$$

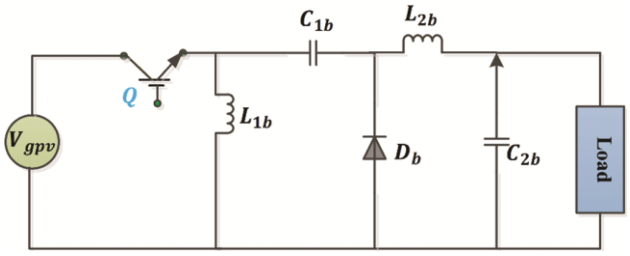

Fig. 7 — The schematic diagram of dc-dc zeta converter

2.3 Design a DC–DC ZETA Converter

Like SEPIC and Cuk converters, the Zeta DC-DC converter is a kind of non-isolated power converter that produces a regulated output voltage that may be greater or lower than the input voltage[23]. It is frequently utilised in battery-powered systems and LED drivers when a constant output current is required. However, the fourth-order DC-DC converters, the SEPIC and Zeta are able to function in both step-up and step-down modes and are not affected by the polarity reversal issue. For the aforementioned application, they are consequently appealing[24]. Zeta converter modelling, also known as SEPIC converter, has never been done or documented in the literature. A two capacitors diode, two inductors and an active power switch make up the fourth-order nonlinear system known as the Zeta converter. Its advantage is Step-up and step-down capability & Continuous input and output current (smoother). The output voltage of the converter is usually controlled by a PWM feedback control loop. A linear model of the converter is required to facilitate stability analysis or feedback control design. A converter for zeta this works models and controls the operation of Continuous Conduction Mode (CCM) a small-signal linear dynamic models of the converter.

The basic zeta converter equivalent circuit diagram as shown in Fig. 7 based on DC-DC Converter & it's a fourth order converter. A zeta converter is similar to BUCK –BOOST Converter but has advantages of having non-inverted output (input- output polarity same). The advantage of zeta converter is reduced input current ripple, Continuous output current, better efficiency than cascaded converters, lower voltage stress on semiconductor components, non-inverting output and lower EMI due to smoother current waveforms

The Converter circuit two modes operating system, mode 1 is switch Q will be close means On-stage the Diode D_b is off with a reverse voltage equal to – (V_{gpv}

+ V_{Ld}), state inductor L_{1b} and L_{2b} are in phase charge. This indicates a linear increase in the inductor's current. The Capacitor C_{1b} will discharge and the energy will charge to V_{Ld} and it is connected in series with L_{2b}. Through Q, the total charging of inductor current passes.

KVL Applying;

$$\frac{di_{L1b}}{dt} = \frac{V_{gpv}}{L_{1b}} \quad \dots (8)$$

$$\frac{di_{L2b}}{dt} = \frac{V_{gpv}}{L_{2b}} + \frac{V_{C1b}}{L_{2b}} - \frac{V_{C2b}}{L_{2b}} \quad \dots (9)$$

By applying KCL, the voltage passing through the capacitors at this pace will be;

$$\frac{dV_{C1b}}{dt} = -\frac{i_{L2b}}{L_{1b}C_{1b}} \quad \dots (10)$$

$$\frac{dV_{c2b}}{dt} = \frac{i_{L2b}}{C_{2b}} - \frac{V_{C2b}}{R_{Ld}C_{2b}} \quad \dots (11)$$

In mode 2 Zeta Converter operating when switch Q is tuning off, the Diode D_b is ON – stage. The Circuit show that the diode is short circuit and Q is open circuit Inductor L_{1b}, that was previous charged will now have to be in discharge. In this stage L_{1b} and L_{2b} are in discharge phase, Since the Voltage Polarity of the inductor changes the diode will get conductL_{1b} and L_{2b} are discharge to capacitor C_{1b} and output part, respectively. As a result, inductor current I_{L1b} *and* I_{L2b} is decreasing linearly.

By applying KVL;

$$\frac{di_{L1b}}{dt} = -\frac{dV_{C1b}}{L_{1b}} \quad \dots (12)$$

$$\frac{di_{L2b}}{dt} = -\frac{dV_{C1b}}{L_{2b}} \quad \dots (13)$$

By applying KCL current flows through the capacitor C_{1b} is express;

$$\frac{dV_{c1b}}{dt} = \frac{i_{L1b}}{C_{1b}} \quad \dots (14)$$

For the zeta converter in CCM, the output and input voltages depend on duty cycle D_{tr}, which is provided;

$$\frac{D_{tr}}{(1-D_{tr})} = \frac{V_{Ld}}{V_{gpv}} \quad \dots (15)$$

Modes one and two below are the resulting equations. It is possible to express the current ripple across the energy-transferring (input) inductor as;

$$L_{1b} = \frac{D_{tr}V_{gpv}}{F\nabla I_{L1b}} \quad \dots (16)$$

It is possible to express the output inductor current ripple.

$$L_{2b} = \frac{D_{tr}V_{gpv}}{F\nabla I_{L2b}} \quad \dots (17)$$

The Capacitor ripples voltages ∇V_{c1} & ∇V_{c2} can be derived from the KCL for 1st and 2nd mode as, F= switching frequency;

$$\nabla V_{C1b} = \frac{1}{C_{1b}}\int_0^{T_{ON}} i_{c1}\, dt \quad \dots (18)$$

$$C_{1b} = \frac{D_{tr}V_{Ld}}{FR_{Ld}\nabla V_{C1b}} \quad \dots (19)$$

$$\nabla V_{C2b} = \frac{1}{C_{2b}}\int_0^{T/2} \frac{\nabla i_{L2}}{4}\, dt \quad \dots (20)$$

$$C_{2b} = \frac{D_{tr}V_{gpv}}{8F^2L_{2b}\nabla V_{C2b}} \quad \dots (21)$$

2.4 Proposed a Switching Reluctance Motor as EV Motors

In a SRM motor, torque is produced by the rotor poles' tendency to align with the excited stator poles. A force generated when a stator coil is energized pulls the rotor to the aligned position. The difference in magnetic reluctance for magnetic field lines between aligned and unaligned rotor positions serves as the foundation for this theory of operation[25]. However, compared to other conventional motors, the issues of acoustic noise and torque ripple are more severe due to the non-linear magnetic features of SRM architecture and its doubly salient poles[26]. The torque ripple is a basic disadvantage of motor drives with switching resistance. The geometric elements that cause the torque ripple include a doubly salient motor, excitation windings in the middle of the stator poles, working modes that need magnetic saturation to maximize the torque per mass ratio, and the pulsed magnetic field created by feeding the different stator windings sequentially. Figure 8 shows the stator and rotor view of SRM 6/4. The primary cause of the torque ripple is phasing current commutation. The SRM motor is selected as an EV motor because of some of its advantages. The stator and rotor have a simple, robust construction with only steel laminations. Avoiding the use of costly, rare-earth minerals, permanent magnets are not necessary. Because of the simple mechanical architecture, it is less costly to manufacture than permanent magnet motors[27] and requires less maintenance. There are no permanent magnets that break down at high temperatures.

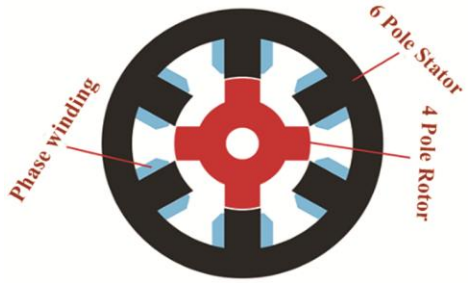

Fig. 8 — The typical structure of 6/4 SRM motors

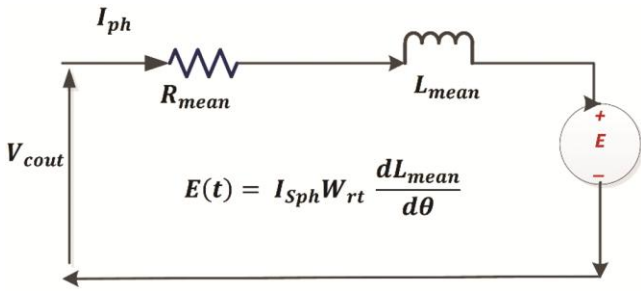

Fig. 9 — The basic equivalent circuit diagram of SRM motors

Outstanding thermal properties since there are no rotor windings, allowing for fault-tolerant operation that can continue even if some phases fail[28]. High beginning torque that is appropriate for accelerating a vehicle broad speed range and high effectiveness. Figure 9 is an equivalent diagram of SRM motor the air gap between the rotor and stator allow for natural cooling & outstanding results in challenging conditions.

Converter output voltage (Vc_{out})

$$Vc_{out} = R_{mean}\, i_{ph} + L_{mean} \frac{di_{ph}}{dt} + i_{ph} \frac{dL_{ph}}{dt} \quad \text{... (22)}$$

$$= R_{mean}\, i_{ph} + L_{mean} \frac{di_{ph}}{dt} + i_{ph} \frac{dL_{ph}}{dt} \times \frac{d\theta}{dt}$$

$$= R_{mean}\, i_{ph} + L_{mean} \frac{di_{ph}}{dt} + W_m\, i_{ph} \frac{dL_{ph}}{d\theta} \quad \text{... (23)}$$

When the rotor poles deviate from the state of alignment, the phase inductance gradually decreases.

Can consider as a back emf as;

$$E(t) = W_m\, i_{ph} \frac{dL_{ph}}{d\theta} \quad \text{... (24)}$$

$$V_{1ph} = Ri_{ph} \frac{d\,\psi}{dt} = Ri_{ph} + \frac{d\,(Li_{ph})}{dt} \quad \text{... (25)}$$

An SRM offers various advantages over other motor types. Applications needing very high speeds can employ the SRM because of its strong structure and lack of rotor windings and permanent magnets. In addition, its rotor inertia is low and it has a good torque/inertia ratio[29]. Since there are no rotor windings or permanent magnets, winding losses occur in the stator. Table 2 shows that the SRM motor parameters consider in the proposed model. In a phase with symmetrically misaligned rotor and stator poles (θ3 – θs), the phase has the lowest inductance (L_{mn}). It's called the unaligned position. The two crucial parts of the controller's reference positions are unsaturated aligned and unaligned incremental inductances. Even if an SR motor or other highly saturated machine disproves the inductance theory.

Table 2 — SRM motor parameters

Parameters	Unit
Power	4.2 KW
Stator pole number	6
Inertia	. 0089 Kg.m^2
Maximum current	10 A
Inductance L_{min}	5.9 mH
Inductance L_{max}	23.6 mH
Stator resistance	3.1 Ω
Rotor pole number	4
Frication	0.01 kg.m/s^2
Maximum flux linkage	0.486 V.s

3 Control Methods of Proposed Model

The flowchart in above Fig. 6 helps to clarify the algorithms thorough execution. The program begins its iterative procedure by acquiring the panel's input voltage (V) and current (I). They are contrasted with values at the conclusion of the previous cycle $(t-1)$ and $(t-1)$. Therefore, the gradual modification is;

$$\Delta V = V(t) - V(t-1) \quad \text{... (26)}$$

The cycle then moves on to the verification of the previously described conditions (Eqs. (5-7)). Due to noise and inaccuracies, Eq. (7) is difficult to meet in practice; hence, the requirement is adjusted with a good approximation by[5];

$$\left| \frac{\Delta I}{\Delta V} + \frac{I}{V} \right| < \varepsilon \quad \text{... (27)}$$

where, ε is a constant positive value, Strategies to minimize torque ripple hysteresis current control ensures the current closely follows the reference, reducing torque ripple. Sinusoidal current shaping shapes the current waveform to minimize ripple. Pulse Width Modulation (PWM) is used to control the current waveform supplied to the SRM phases. Adjusting the turn-on and turn-off angles of each phase can improve torque smoothness. Non-linear commutation techniques optimize excitation timing based on rotor position and load conditions.

3.1 Implement ADITC Technique

Switched Reluctance Motors are widely used in industrial and automotive applications due to their simple structure, robustness, and cost-effectiveness. However, torque ripple and efficiency remain significant challenges in SRM control. ADITC technique is an advanced control strategy designed to minimize torque ripple, enhance efficiency, and improve dynamic performance.

ADITC's control system is depicted in Fig. 10, where $D_t(k)$ denotes the incoming phase and $D_t(k-1)$ the outgoing phase. X-axis represents torque error, while y-axis represents $D_t(k)$ and $D_t(k-1)$ switching states.

Take use of PWM's ability to change the phase winding's average voltage from 0 to V_{Hpv} in a single sampling period. Additionally, the control system no longer uses the hysteresis rule. Now, the duty ratio of PWM allows the current state to choose the phase state between states 0 and 1. The duty ratio of switching modes is determined by the torque error, the phase incoming and outgoing shown in Fig. 11. This is how DTR is written:

$$D_{tr} = Ab_s\left(\frac{T_{err}}{\nabla T_H}\right) \quad \ldots (28)$$

where;

∇T_H is torque bandwidth, T_{err} is torque error,

The ADITC block diagram is shown in Fig. 12. An ADITC controller and a PWM generator take the role of the hysteresis controller. In a single sampling time, the ADITC approach may control a range of phase currents by changing the average phase voltage. This can lengthen the sampling period and reduce torque ripple. because basic hysteresis switch principles are used in the traditional DITC approach[30]. Based on the torque inaccuracy at each sample interval, only one phase state is used. The torque variation with load torque and speed at full DC-link voltage is shown in Fig. 12. One way to make sure the torque ripple remains within a range is to shorten the sampling period, which raises hardware expenses.

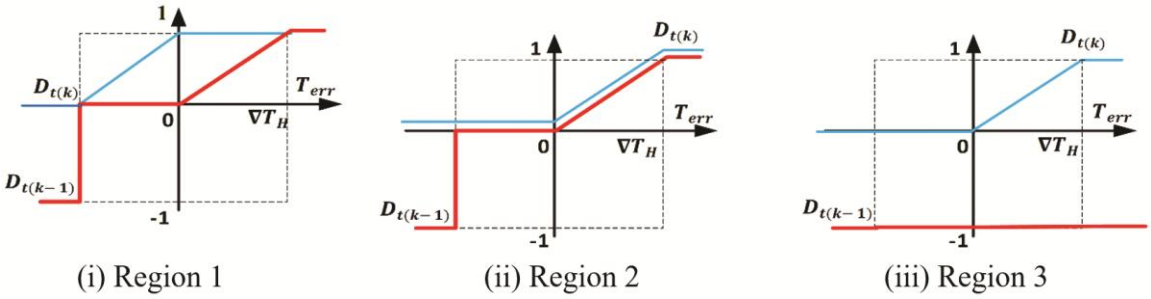

Fig. 10 — The asymmetric converter's ADITC scheme

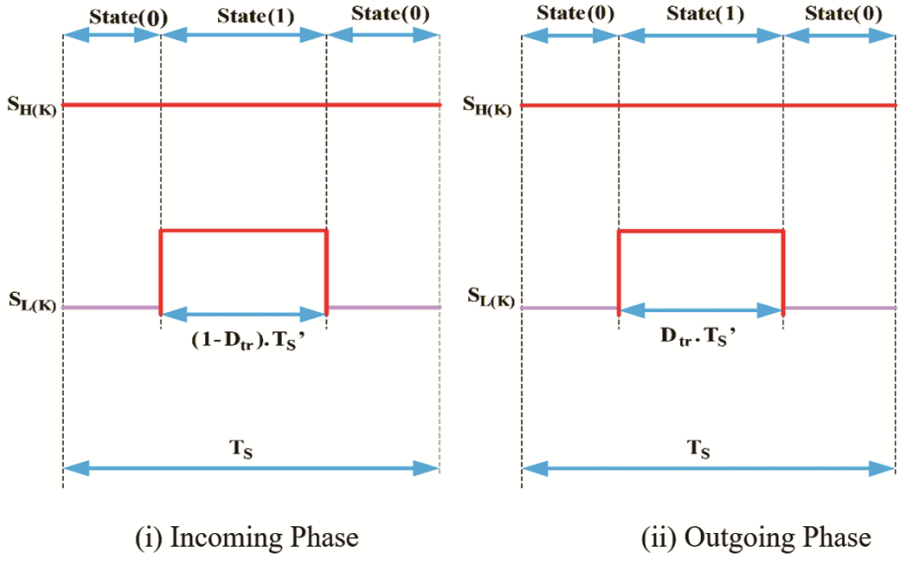

Fig. 11 — Changing the incoming and outgoing phase modes

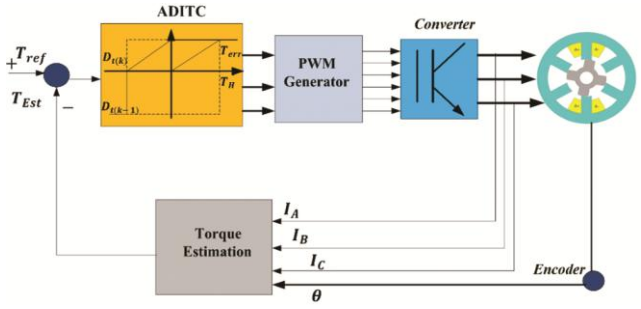

Fig. 12 — Controlling parts of block diagram in ADITC technique

Another is to regulate the phase winding's average voltage while sampling. the choice to employ the PWM method.

4 Results and Discussion

The proposed model focuses on the application of sunroof electric vehicles. First, discuss a set of PV panels under different atmospheric conditions to evaluate their performance and the maximum power achieved using MPPT. To aim to minimize voltage and current ripple in the output graphs; to achieve this; it utilizes a Zeta Converter along with an ADITC technique. There are two ways to ensure that torque ripple remains within an acceptable range. First, the production of power from solar roofs in different atmospheric circumstances. By directly controlling instantaneous torque, to eliminate the need for a current controller, thereby reducing torque ripple and enhancing dynamic response. This gives ADITC several advantages over indirect instantaneous torque control. An ADITC-based adaptive commutation approach is recommended for switched reluctance motors. This control strategy is promising for SRM drives, particularly in electric vehicle applications, as it effectively reduces torque ripple while significantly improving motor efficiency through intelligent adjustments.

4.1 Solar Roof Performance

The Figs. 13-14 show that the voltage and current graph of a PV array output and Zeta converter output at the irradiance 500 W/m^2 and temperature 25 ^{0}C. The using PV array its ripple is less by using INC MPPT technique. The sky is overcast. When seen in the accompanying image, our suggested model's reaction decreases when the solar cell absorbs less light. Following the PV array, it's linked the control method to smooth out the power supply to the EV battery and eliminate ripple by up to 40 % of the solar cell's output.

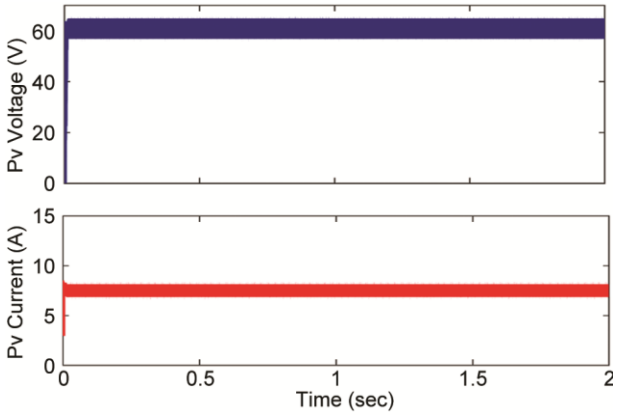

Fig. 13 — The simulation results of PV array of an irradiance 500 W/m²

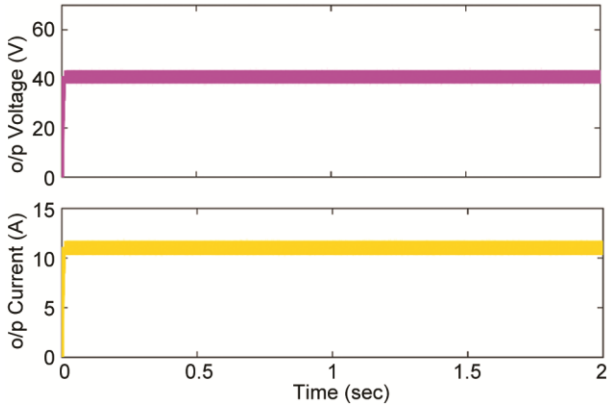

Fig. 14 — The simulation results outcome from zeta converter at irradiance 500 W/m^2

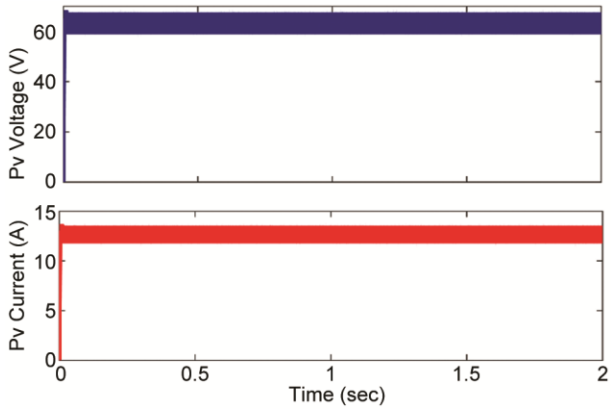

Fig. 15 — The simulation results of PV array of an irradiance 1000 W/ m^2

The Figs. 15-16 show that the voltage and current response of a PV array output and Zeta converter output at irradiance 1000 W/m^2 and constant temperature 25 °C. In the PV array model, the maximum solar energy outcome occurs at maximum

irradiance; in this situation, the PV array operates at maximum efficiency to produce power.

Table 3 shows that the average power output of solar roof panels is supplied to the system at different atmospheric conditions; it's clear that the solar roof power supply average is 594 watts. Now the next part discusses the Li-ion battery connected to our proposed dynamic EV model.

4.2 Discussion About a Li-ion Battery Consider

Now discuss battery parameters shown in Table 4 of the SRM motor run in the 5 hr range without the solar roof added, then the running time of the SRM motor increases depending upon atmospheric conditions. The EV motor is directly attached to the battery, as in Fig. 17. The battery discharges at a rate of 0.0444 % of SoC each 10 seconds, or 0.00444 % per second. It takes five hours in total to reach DoD 80 %. Run EVs have a 4.2 kW SRM motors, a 546 Ah battery, 100 % SoC at first, and a nominal 48 V Li-ion battery voltage at 20 % drain.

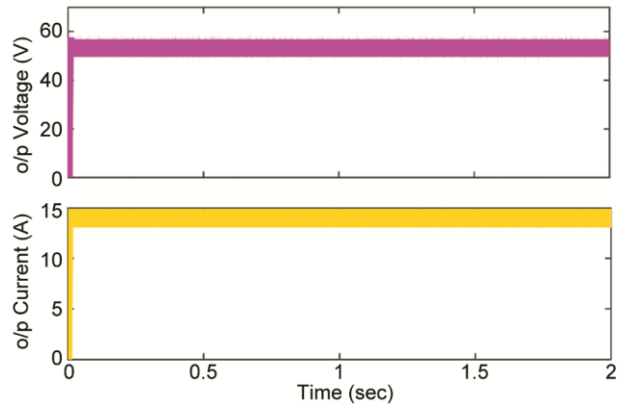

Fig. 16 — The simulation results of Zeta Converter of an irradiance 1000 W/ m^2

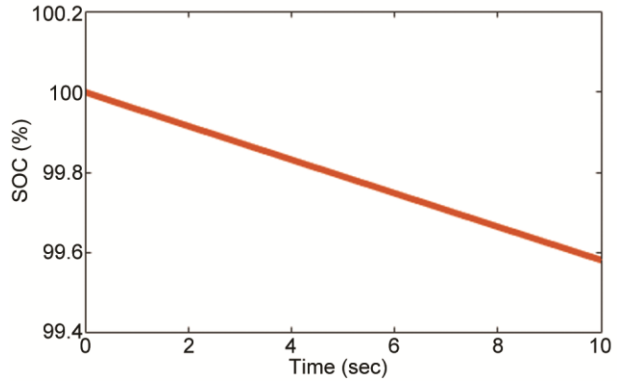

Fig. 17 — Li-ion battery response without solar roof connected discharge rate of a battery

Figure 18 displays the SoC reaction. For operating an EV SRM motor with a solar roof, it is shown that the discharge rate is 0.0368 % SoC every 10 seconds if the system connects the lithium battery to the solar roof power source. Discharge rate with solar roof is 0.00368 % per sec. of a SoC. It means the running time of the EV motor is increased by 1 hr 2 min by the integrated with PV array.

4.3 Now Discussion About Torque Ripple by Apply ADITC Technique

Advanced torque estimating algorithms that take into account the motor's magnetic properties, rotor position, and phase currents are commonly used in the ADITC technique. In order to respond quickly to changes in torque, these estimations are updated at high frequencies. The system has a multi-level control

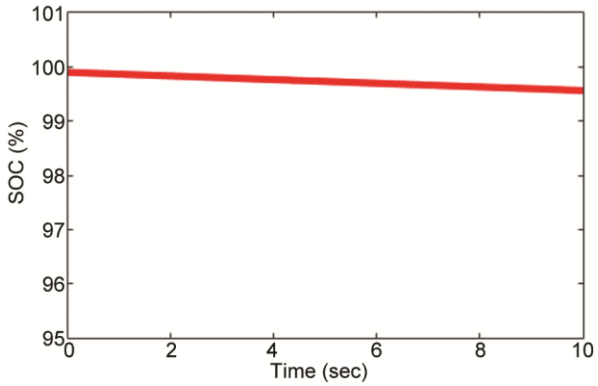

Fig. 18 — Li-ion battery response with solar roof connected discharge rate of a battery

Table 4 — The Li-ion battery specification

Parameters	Units
Maximum Capacity	546Ah
Nominal Voltage	48V
Initially SoC	100%
Depth of Discharge (DoD)	80%
Cut of Voltage	36V
Internal resistance	0.563Ω

Table 3 — PV Array to Out power outcome at different Irradiance

Irradiance (W/m^2)	PV Array Response		Converter Response		Output Power(W)
	Voltage o/p (V)	Current o/p (A)	Voltage o/p (V)	Current o/p (A)	
500	58.58	7.62	38.54	10.52	405.44
750	62.04	9.23	41.64	13.54	563.81
1000	67.56	12.71	56.62	14.37	813.63

structure, with inner loops handling the switching sequences and the outside loop managing the torque reference. Phase controllers and hysteresis controllers are frequently combined to maximize switching choices. To guarantee seamless torque shifts, ADITC synchronizes several stages.

Overlapping conduction techniques aid in sustaining constant torque generation and lowering ripple amplitude during commutation periods. In the graph above displays the torque response of an SRM EV motor implemented using a suggested control technique. Figure 19 illustrates the torque ripple that exists when there is no mechanical load; Fig. 20 displays the torque ripple graph when there is half load; and Fig. 21 displays the suggested system operating at rated load, followed by the torque ripple reaction as displayed in the graph above. The SRM motor operates; the torque ripple minimum and maximum are the two spots chosen for torque response during the EV motor's operation for each load state. The average torque ripple for each of the three scenarios is now being discussed.

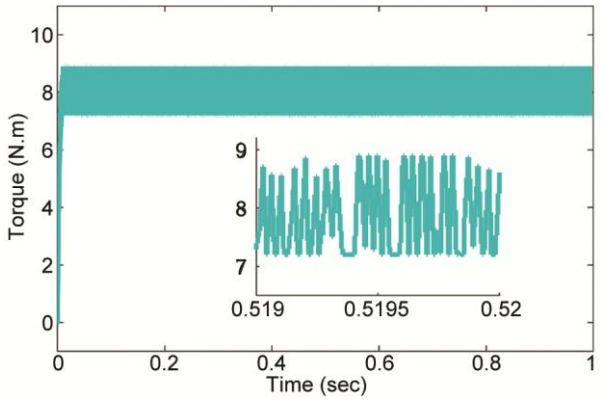

Fig. 19 — The torque response ripple is presented a graph under no-load conditions

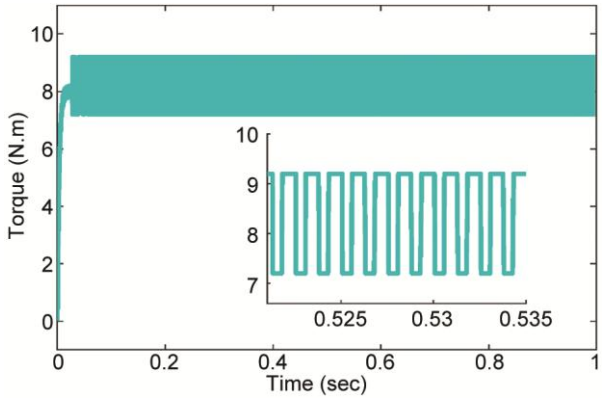

Fig. 20 — The torque response ripple is presented a graph under half-load conditions

It is evident from Table 5 that the torque ripple is reduced as the load increases when the ADITC approach is applied. Recent studies show that modern ADITC implementations can achieve torque ripple values of 20–30 %, which is significantly better than traditional control strategies like IIITC and DTC, which frequently show torque ripple of 40–50 %; at no load condition, it ranges from 30 % to 60 %; at half load, it ranges from 25 % to 45 %; and at full load, it ranges from 20 % to 30 %.

In the Fig. 22 show that the 3D Plot as axis defined the y- axis is a load torque, x- axis is generating torque and z-axis is the torque ripple generated by varies the load condition. The high speed, low torque is generated the less ripple.

4.4 Now Speed Response of SRM Motor is Under All Three Conditions

The motor requires very little torque to run at its top speed. The switching frequency and the back EMF effects are the main factors limiting speed. At low speeds, speed-torque characteristics exhibit consistent performance; as speed increases, there is a tiny droop. Features of switched reluctance in a 6/4

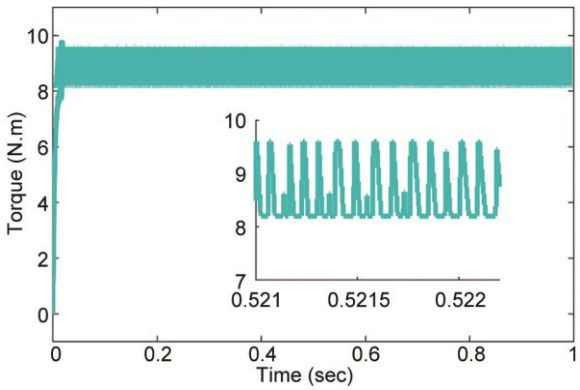

Fig. 21 — The torque response ripple is presented a graph under rated-load conditions

Table 5 — The EV SRM motor implement ADITC techniques the torque ripple in different load condition

Condition	Average Torque Gen. (N.m)	Speed (rpm)	Average Torque Ripple (%)
Light Load	7.75	4950	12.47
Half Load	8.42	4460	13.29
Full Load	9.46	3860	11.62
DTC (Rated load)[31]	10.2	4000	32.39

excitation angle-driven motor with minimal current consumption and excellent efficiency, the motor runs in the middle of its torque-speed characteristic curve, and speed drops when compared to no-load operation because of the increased torque demand. As the motor generates its rated torque, the operating point moves to the lower speed zone of the torque-speed curve, resulting in the maximum speed reduction.

In EV system, choosing the SRM motors requires an understanding of the speed-time profile under various loads as shown in Fig. 23. It guarantees that, even with rated or fluctuating loads, the system will reach the necessary speed in the acceptable amount of time. The steep starting slope of all curves indicates strong acceleration right after start-up. This area is highlighted by the term "Accelerate" and the corresponding arrow. As the system gets closer to its ultimate speed, the acceleration rate steadily drops from its peak at the beginning. Each curve asymptotically approaches a constant speed over time; this is denoted by the green "Saturation" mark. As the load increases, this saturation value falls:

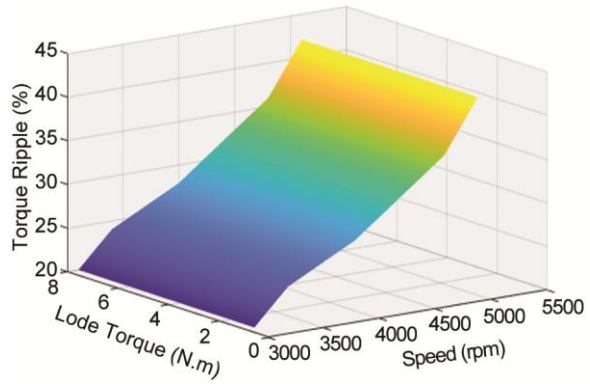

Fig. 22 — The 3D Surface plot graph of speed, load torque, and torque ripple

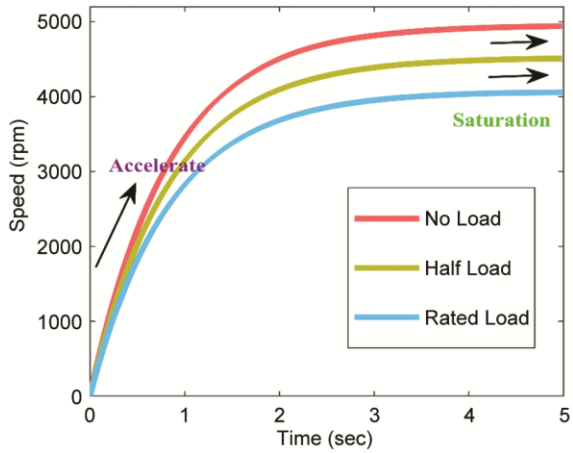

Fig. 23 — Speed response of proposed dynamic EVs system

4.5 OPAL-RT Real-Time Simulator for Hardware Validation

The OPAL-RT real-time simulator (OP4512) in the RT lab has been used to implement the suggested method and validate the results. The model was created in MATLAB/Simulink on a desktop computer in an RT lab (Intel Core i7-8700 CPU @ 3.40 GHz 3.19 GHz, RAM 8.0 GB, 64-bit operating system) for verification. A 16-channel digital-to-analogue card (DAC) with a 4-channel, 100 MHz digital oscilloscope (DSO X3034T). Figure 24 shows how the OPAL-RT laboratory is set up for real-time verification, Fig. 25 (a) the show the torque ripple of DTC controller, (b) shown advance DITC controller results of torque generation its ripple is minimise up to 59.68 % of the tradition method as show in Fig. 25 (b). Nevertheless, these outcomes are shown in Fig. 26 is prior to executing the suggested model in a real-time OPAL-RT simulator.

In the above graph shows that the torque response of running SRM motor during half load condition in this graph the present torque ripple, the oscilloscope range set up 0 – 15 unit in our torque response show approximate 7.2 – 8.5N.m, as it appears in the MATLAB simulation, which confirms the OPAL-RT finding.

A quantitative comparison of torque ripples percentages for three distinct control strategies basic controller, traditional controller, and implementation of ADITC across a range of load applications are shown in Figure. 26 shown clearly demonstrates that the ADITC method has a much better performance compared to regular DTC for the purpose of minimizing torque ripple. Unlike the regular DTC

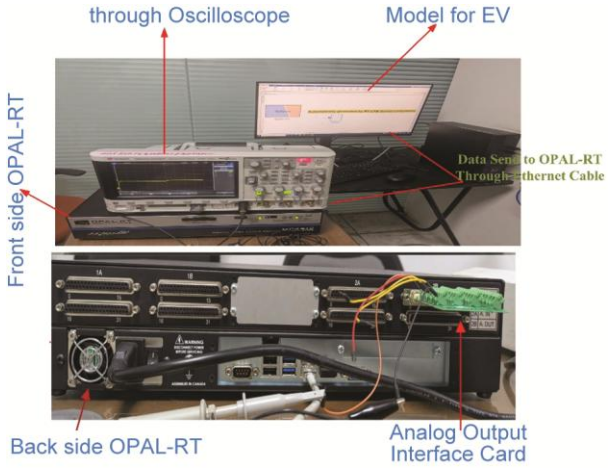

Fig. 24 — RT-Lab's OPAL-RT real-time simulator is set up for the suggested model's validation

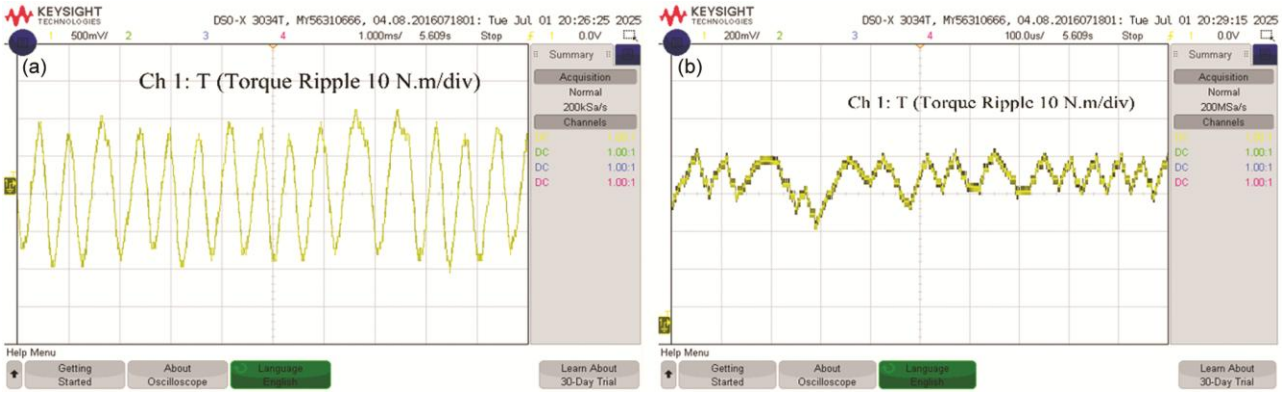

Fig. 25 — OPAL-RT real time simulation results: (a) the torque ripple representation of a DTC control technique; and (b) by implements advance DITC technique to control torque ripple

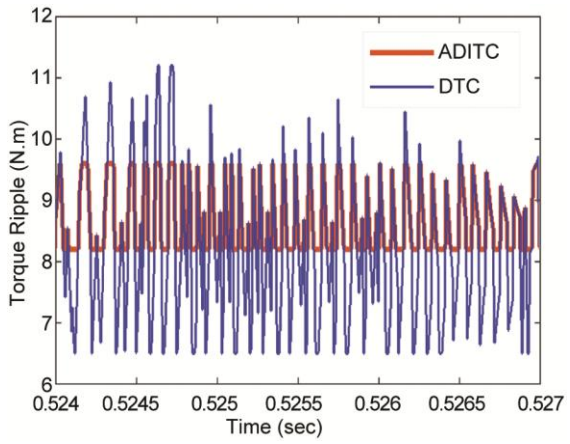

Fig. 26 — The different controller performance with respect to load apply

which has irregular stochastic disturbances with a very high torque ripple ratio of 56 %, ADITC limits the torque to a periodic range within 8.3 - 9.6 N.m, thereby reducing the load torque ripple by 13 %. As a result, it leads to a remarkable 70 % reduction in the torque ripple ratio.

5 Conclusion

A proposed solar roof model for electrical vehicle is better running condition as compare to normal EV cars. The using MPPT based PV array to achieve maximum power also using Zeta Converter Voltage and current fluctuation is minimise thus by power supply is smooth. By apply sunroof the running time is increase by 1hr 2 minute extra added on Battery capacity, its means 20.66 % raise every one complete discharge the battery. Normally Discharge Rate of Battery is 0.0444 % of SoC / Sec but adding Sunroof Discharge Rate is 0.0368 % of SoC / Sec. ADITC is a highly effective control technique for SRM motors, offering superior torque control, higher efficiency, and improved dynamic response compared to conventional methods. In this technique different load condition torque ripple is varies in percentage of approximate 11.6 % to 13.3 %. The Speed response of SRM EV Motor is very smooth ripple is very less is may be negligible. The speed is to take a time to accelerate up to 4000 rpm in 1.5 - 2.0 sec under no load to full load condition. These initiatives seek to improve solar roof EV systems' sustainability, dependability, and efficiency. Future studies could examine the creation of resilient semiconductor materials or creative defences to improve system dependability. Proposed MATLAB simulation model also Verify by OPAL- RT real time simulator. System efficiency could be further increased by adjusting battery characteristics and looking at more sophisticated control techniques outside of ADITC. Performance monitoring and management skills could be improved by IoT-based monitoring systems. In future study also addresses design challenges including weight optimization, thermal management of roof-mounted solar cells, and advanced power electronics for seamless integration between solar generation and SRM drive systems.

Reference

1 Boumaalif Y, Ouadi H & Giri F, *IFAC- Papers*, 58 (13) (2024) 703.
2 Kumar V & Hote V Y, *IFAC J Syst Control*, 31 (2025) 100295.
3 Qi qiang Guan, Hongxin Zhang, Jian Yang & Jie Zhou, *J Renew Sustain Energy*, 17 (6) (2025) 064103.
4 Deepak M & Janaki G, *Int J Circuit Theory Appl*, 52 (7) (2024) 3213.
5 Rhimi Z, Hamed M, Fellah A, Ghernaout D, Kriaa K & Elboughdiri N, *J Renew Sustain Energy*, 17 (6) (2025) 063702.
6 Mazumdar D, Guerrero J M, Sain C & Ustun T S, *J Renew Sustain Energy*, 17 (4) (2025) 046306.

7 Patel N, Sovetkin E, Pieters B, *et al.*, *Prog Photovolt Res Appl*, 33 (2025) 616.
8 Narayana V, Mishra A K & Singh B, *IET Power Electron*, 10 (2) (2017) 156.
9 Yong Li, Adeleke O P & Xu X, *J Renew Sustain Energy*, 11 (6) (2019) 062701.
10 Padmanaban A L & Saravanan P, *Automat*, 64 (2023) 239.
11 Kurian S & Chellappan V, *Emerg Trends Mech, Springer*, (2024) pp.167-185.
12 Diao K, Sun X, Bramerdorfer G, *et al*; *Renew Sustain Energy Rev*, 168 (2022) 112785.
13 Benqin J & Benqin D, *Adv Electr Machines Drives Technol*, 11 (2) (2023) 179.
14 Sahu N & Panda A K, *J Electr Syst Inform Technol*, 5 (3) (2018) 829.
15 Youn H, Kim G & Ban J, *Int J Control Autom Syst*, 23 (2025) 674.
16 Abdel-Kader F E S, Elsherif M Z, Abdel-Rahim N M B & Fathy M M,*J Renew Sustain Energy*, 4 (6) (2012) 063142.
17 Mohamed A, Ahmad R & Xavier B, *IET Smart Grid*, 7 (6) (2024) 904.
18 Hepzibah A A & Premkumar K, *Electr Eng*, 102 (2020) 421.
19 Tiwari R & Maurya R, *Int J Circuit Theory Appl*, 54 (3) (2026) 1785.
20 Mishra A & Singh B, *Int J Emerg Electr Power Syst*, 19 (5) (2018), https://doi.org/10.1515/ijeeps-2018-0028.
21 Mishra A & Singh B, *IEEE Trans Indust Inform*, 17 (1) (2021) 290.
22 Jeremy L J, Ooi C A & Teh J, *J Renew Sustain Energy*, 12 (1) (2020) 013502.
23 Banaei M R & Bonab H B, *IEEE Trans Indust Electron*, 67 (3) (2020) 1991.
24 Chen Y T, Lu Z X & Liang R H, *IEEE Transact Power Electron*, 33 (1) (2018) 425.
25 Saleh A L, Amyal AL F & Sz´amel L, *AIMS Electron Electr Eng*, 8 (2024) 104.
26 Mukhopadhyay S, Mansani S & Sekaran S, *Electr Eng*, 106 (2024) 7035.
27 Damarla I, Vadlamudi B, Mahendran V & Rao K, *Int J Circuit Theory Appl*, 53 (2024) 2718.
28 Kakodia S K & Dyanamina G, *Int J Circuit Theory Appl*, 50 (10) (2022) 3426.
29 Dutta A, Das S S & Panda A, *Int J Circuit Theory Appl*, 52 (10) (2024) 5184.
30 Kannan R, Rajasekaran S, Stallon D & Anand R, *ISA Trans*, 139 (2023) 322.
31 Quraan A l & Szamel L, *IET Electr Power Appl*, 17 (12) (2023) 1502.